Biologically Inspired Design Of Small Flapping Wing Air Vehicles Using Four-Bar Mechanisms And Quasi-steady Aerodynamics

Rajkiran Madangopal
Graduate Student
e-mail: madangop@me.udel.edu

Zaeem A. Khan
Graduate Student
e-mail: khanza@me.udel.edu

Sunil K. Agrawal
Ph.D.
Professor
e-mail: agrawal@me.udel.edu

Mechanical Systems Laboratory, Department of Mechanical Engineering, University of Delaware, Newark, DE 19716

In this paper, the energetics of a flapping wing micro air vehicle is analyzed with the objective of design of flapping wing air vehicles. The salient features of this study are: (i) design of an energy storage mechanism in the air vehicle similar to an insect thorax which stores part of the kinetic energy of the wing as elastic potential energy in the thorax during a flapping cycle; (ii) inclusion of aerodynamic wing models using blade element theory and inertia of the mechanism using rigid body modeling techniques; (iii) optimization of parameters of the energy storage mechanism using the dynamic models so that the peak power input from the external actuators during a flapping cycle is minimized. A series of engineering prototypes based on these studies have been fabricated which justify the use of these mathematical techniques. [DOI: 10.1115/1.1899690]

Introduction

In the last five years, funded by programs from DARPA and other DoD agencies, the area of micro air vehicles (MAVs) has seen a spurt of research activities. Microbats, with 6–8 in. wing span and weight under 15 g, were designed to fly remotely via radio control [1]. A helicopter-like MAV, called mesicopter, weighing 15 g was developed that uses miniature rotorcraft technology. Mentor, a hovering MAV with a biplane wingset, was shown to be stabilized successfully by moveable fins on the lower part of the fuselage [2]. A micromechanical flying insect, 10–25 mm wingtip to wingtip, has been proposed recently. Even though these MAV developments are impressive, the field of flapping wing MAVs is still in its infancy. Each one of these designs is unique and cleverly utilizes a specific aerodynamic principle. However, at this time, a systematic design philosophy for a range of flapping wing MAVs is lacking.

The conventional aerodynamic analysis of animal flight invokes the *quasi-steady assumption* to reduce a problem in dynamics to a succession of static conditions. It is assumed that the instantaneous forces on flapping wings are equivalent to those for steady motion at the same instantaneous velocity and angle of attack. It is generally believed that the quasi-steady assumption is valid for fast forward flight because of the low value of the reduced frequency parameter (the ratio of the flapping velocity of the wings to the forward flight velocity). At low values, the steady flight velocity dominates the flow over the wings and reduces the spatial derivatives of the fluctuating aerodynamic parameters. Thus, the unsteady aerodynamic effects are small compared to quasi-steady ones [3]. The usual aerodynamic treatment of animal flight is based on the *blade element theory* of propellers developed by Drzewiecki [3]. The fundamental unit of analysis is the blade or a wing element which is that portion of a wing between the radial distances y and $y+dy$ from the wing base (or root). This theory relies on the successive step-wise solutions of equations for the sectional lift and thrust forces. Complete kinematic data are necessary for this approach. The motion of the longitudinal axis of the wing, the geometric angle of attack and the section profile must all be known as functions of time and radial position [3].

Contributed by the Mechanisms and Design Committee for publication in the JOURNAL OF MECHANICAL DESIGN. Manuscript received: May 25, 2004; revised: October 4, 2004. Associate Editor: G. R. Pennock.

With recent advances in computational fluid dynamics (CFD), efforts in mathematical modeling of insect flight have moved away from quasi-steady approximations to full scale Navier-Stokes simulations of fluid dynamics. However, while CFD models show promise as an important tool, their application to insect flight is as yet limited by the complex nature of three-dimensional flows in intermediate-to-low Reynolds number and by conventional resourses required to simulate such conditions. Although not as rigorous as computational simulations, quasi-steady models continue to offer a tractable means of calculating instantaneous forces from measured kinematics. These models are readily applicable to the analysis of energy and power requirements and are more easily incorporated into dynamic control models of insect flight [4].

An insect's thorax, to which the wings are attached, is packed with a complex of flight muscles, together with various other structures for coupling and operating the wings. It is from here that all the power and control emanates, enabling the insect to carry out almost any aerial maneuver [5]. The thorax can be considered simply as an elastic box with a lid (called the tergal plate) on top. Two types of flapping mechanisms are found in most insects, *direct* and *indirect*, as shown in Fig. 1.

In the direct flapping mechanism, found in dragonflies and grasshoppers, the flight muscles are attached directly to the wing levers on each side of the pivot. Alternate contraction of these muscles brings about the flapping motion. In this mechanism, the wing amplitude for each wing can be varied independently. In the indirect flight mechanism, found in bees and flies, the two pairs of muscles are connected to the walls of the thorax and not attached near the wing's base. The up and down motion of the tergal plate brings about the flapping motion.

The point to note regarding these flapping mechanisms is that they represent an oscillating system with high elasticity. The wings, at the end of each stroke, need to stop and reverse direction. At the end of each stroke, the kinetic energy of the wings is stored as elastic potential energy in the walls of the thorax and this energy is released during the subsequent stroke [6]. Flapping wing motion is not a planar motion. During one complete cycle of flapping, the wings undergo spanwise twisting due to which at each instant the relative angle of attack changes so as to generate suitable ratios of lift and thrust during a cycle.

Our research on mechanical flapping wing air vehicles is inspired from flying behavior of (i) larger insects, the hawkmoths

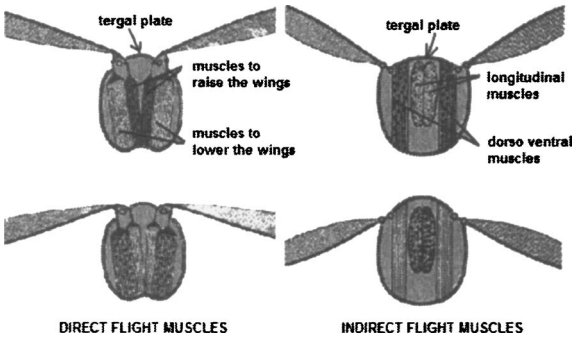

Fig. 1 Flapping mechanisms in insects (courtesy: Hooper Virtual Paleontological Museum)

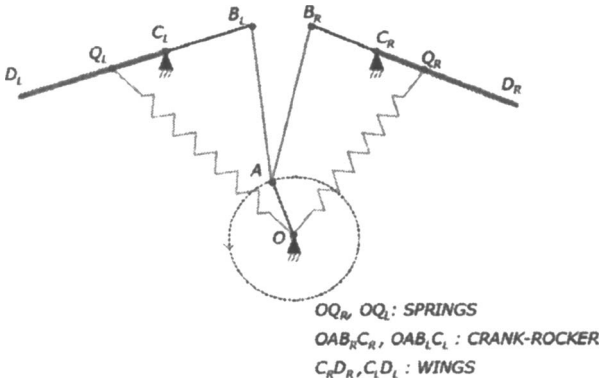

Fig. 4 A simple flapping mechanism

and (ii) smaller birds, the hummingbirds. Over the last two years, we have fabricated a series of motor driven flapping wing small machines, which have successfully flown outdoors. Our earliest successful prototype was made out of balsa wood, weighed 50 grams, and had a wing span of 50 cm. Our new designs are made out of lightweight carbon fiber composites, weigh 15 grams, and have a wingspan of 36 cm. These prototypes are shown in Fig. 2. Snapshots from a sample motion of these prototypes are shown in Fig. 3.

In this paper, we have proposed a simple mechanical flapping mechanism based on ideas obtained from the study of insect and bird flight and the knowledge gained from test flying our prototypes. We begin with the kinematic model of the mechanism in the next section. In the following section, we motivate the energetics-based design and describe the rigid-body dynamic model in which the equations of motion are derived. This follows with a section on an aerodynamic model which gives expressions for lift, thrust and aerodynamic moment. The last section deals with the optimization of the design in which we make use of the energetics in the system to reduce the peak input power required to drive the system.

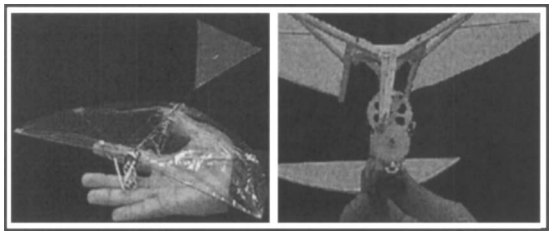

Fig. 2 Prototypes of birds with high speed flapping wings

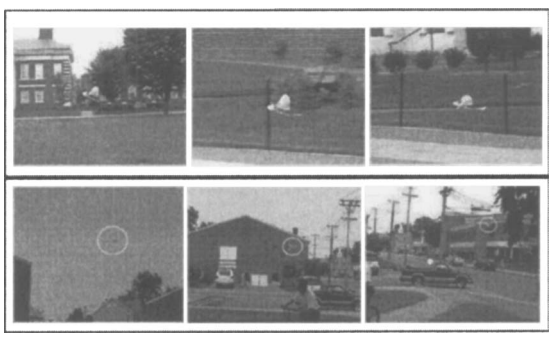

Fig. 3 Prototypes in flight

1 Kinematic Model

In order to analyze the energetics of a mechanical flapping wing mechanism, we have captured some of its essential attributes shown in Fig. 4. The system has two planar four bar mechanisms, both of which are driven by a single crank OA. The vehicle is powered by an electric motor through a gear box to reduce speed. The wings C_RD_R and C_LD_L are pivoted at the fixed points C_R and C_L respectively. The tergal plate lid is replaced by two four bar mechanisms OAB_RC_RO and OAB_LC_LO which bring about the flapping motion. The direct flight musles are approximated by two tension springs OQ_R and OQ_L, each of which is connected to a wing.

The parameters of the system are crank length l_1, coupler length l_2, rocker length l_3 and the wing length l_4 (see Fig. 5). We select the point of attachment of the tension springs, i.e., Q_R and Q_L along the wings' leading edges C_RD_R and C_LD_L, respectively. The lengths C_RQ_R and C_LQ_L are represented by the variable r. Knowing the angular displacement of the crank θ_1, the angular displacements of the coupler θ_2 and the rocker θ_3 can be obtained in terms of θ_1 using vector loop closure $O-A-B_R-C_R-O$ (see Fig. 5).

$$\mathbf{r}_{OA} + \mathbf{r}_{AB} + \mathbf{r}_{BC} = \mathbf{r}_{OC} \tag{1}$$

$$l_1 \cos\theta_1 + l_2 \cos\theta_2 + l_3 \cos\theta_3 = d_x \tag{2}$$

$$l_1 \sin\theta_1 + l_2 \sin\theta_2 + l_3 \sin\theta_3 = d_y \tag{3}$$

A similar vector loop can be written for $O-A-B_L-C_L-O$ (see Fig. 6) to determine $\theta_4(\theta_1)$ and $\theta_5(\theta_1)$. Figure 7 shows the range of motion of the wing during a cycle of flapping motion.

The velocities of the crank, coupler and rocker are derived as follows. The bird is inertially fixed and is oriented at a constant pitch angle $\bar{\theta}_a$ relative to earth (see Fig. 9). The frame attached to

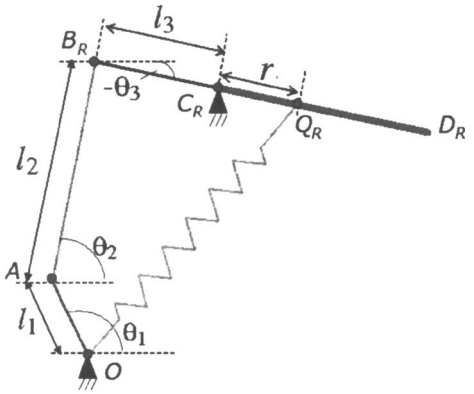

Fig. 5 Parameters of the mechanism

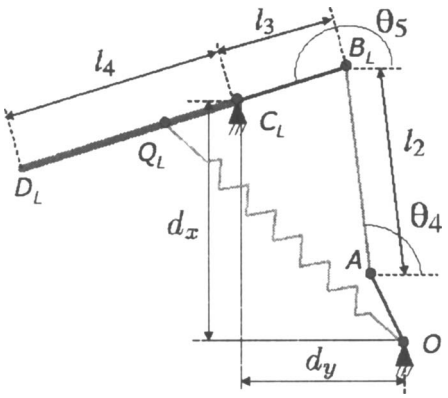

Fig. 6 Second four-bar mechanism. Note that the lengths d_x and d_y are the same for both four-bar mechanisms

the bird is $(\hat{\mathbf{x}}_b, \hat{\mathbf{y}}_b, \hat{\mathbf{z}}_b)$ and those attached to the crank, coupler and rocker are: $(\hat{\mathbf{x}}_1, \hat{\mathbf{y}}_1, \hat{\mathbf{z}}_1), (\hat{\mathbf{x}}_2, \hat{\mathbf{y}}_2, \hat{\mathbf{z}}_2)$ and $(\hat{\mathbf{x}}_3, \hat{\mathbf{y}}_3, \hat{\mathbf{z}}_3)$ respectively for the chain OAB_RC_RO as shown in Fig. 8. Let the links be represented by subscript i with the values 1 for the crank, 2 for the coupler, and 3 for the rocker.

The transformation from the earth frame to the bird frame can be represented by the fixed rotation matrix

$$R = \begin{pmatrix} 1 & 0 & 0 \\ 0 & \cos\bar{\theta}_a & -\sin\bar{\theta}_a \\ 0 & \sin\bar{\theta}_a & \cos\bar{\theta}_a \end{pmatrix} \tag{4}$$

Note that the attitude of the bird is considered to be fixed in the inertial reference frame. Referring to Fig. 7, the angular velocities of the links can be written as

$$\omega_1 = \dot{\theta}_1 \hat{\mathbf{z}}_1, \tag{5}$$

$$\omega_2 = \dot{\theta}_2 \hat{\mathbf{z}}_2, \tag{6}$$

$$\omega_3 = \dot{\theta}_3 \hat{\mathbf{z}}_3. \tag{7}$$

The velocities of the center of masses G_i of the links can be written as

$$\mathbf{V}_{G_i} = \mathbf{V}_X + \omega_i \times \mathbf{r}_{XG_i}, \tag{8}$$

where $X=O$ for the crank, $X=A$ for the coupler, and $X=C$ for the rocker. Similar expressions can be written for the links making up the loop $O-A-B_L-C_L-O$. On using the geometric relations $\theta_i = \theta_i(\theta_1)$, $i=4, 5$, we can write all the velocities in terms of θ_1 and ω_1.

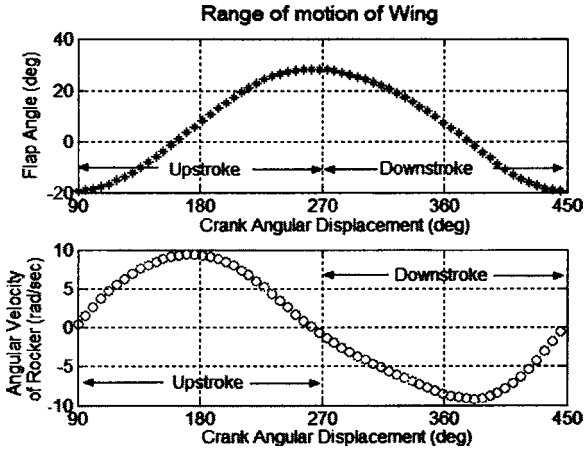

Fig. 7 Range of motion of the wing. The values of the parameters used are shown in Table 1

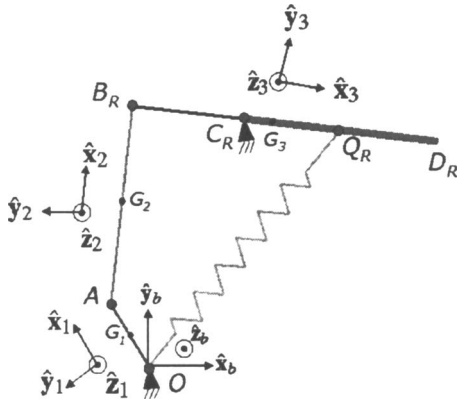

Fig. 8 Frames attached to the links

2 Energetics and Rigid Body Dynamics

In flapping wing mechanisms, the aerodynamic forces are considerable during motion. These forces cause an aerodynamic moment to be overcome by the motor in order to maintain the required lift and thrust. The magnitude of the aerodynamic forces (moment) during the downward power stroke is greater than during the upstroke. At the end of the upstroke or downstroke, the wings decelerate to zero speed causing the aerodynamic moments to vanish. At the start of the next stroke the wings need to accelerate from rest. The consequence of this phenomenon is that the motor experiences *shock*, or varying torque during a cycle.

Insects overcome this problem by storing the kinetic energy of the wings as elastic potential energy in the thorax and this energy is released in the subsequent stroke so that the work done by the muscles is reduced. Taking a cue from the insects, we have incorporated springs into the design. These springs are tension springs, which are attached to the leading edge of the wings as shown in Fig. 4. The springs are so attached that they are unstretched during the start of the upstroke and fully stretched at the end of the upstroke (or beginning of the downstroke). Hence, they pull the wings down thereby aiding the motor and reducing the load torque. In this manner, the variation in load torque acting on the motor during one complete cycle is reduced. In this study, we have assumed that the crank rotates at constant angular velocity. Hence, a reduction in the variation of the load torque is proportional to a reduction in the variation in the peak input power required to drive the system.

The kinetic and potential energies of the links are given by the following expressions. The total kinetic energy of the crank, the coupler and the rocker of each wing is the sum of the rotational as well as translational kinetic energies and can be given by the general expression,

$$K_i = K_{T_i} + K_{R_i} \tag{9}$$

where,

$$K_{T_i} = \frac{1}{2} m_i \mathbf{V}_{G_i} \cdot \mathbf{V}_{G_i}, \tag{10}$$

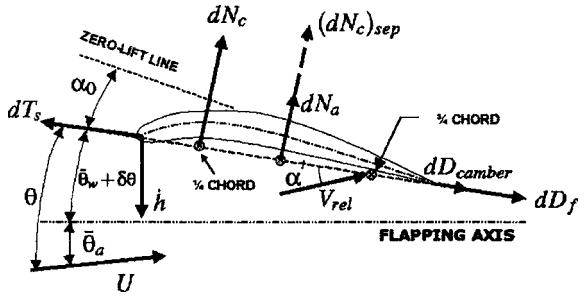

Fig. 9 Wing section showing aerodynamic forces and moments

$$K_{R_i} = \frac{1}{2}\omega_i \cdot I_{G_i} \cdot \omega_i. \tag{11}$$

Here, m_i is the mass of link i and I_{G_i} is the mass moment of inertia of link i about its CG. The potential energy of the links is given by the general expression,

$$P_i = m_i g h_i, \tag{12}$$

where h_i is the height of the center of mass of link i from the crank center O.

The energy stored in each spring is given by the expression

$$U_{s_i} = \frac{1}{2}k_{s_i}\delta_i^2, \quad i = 1,2 \tag{13}$$

where k_{s_i} is the stiffness of the spring and δ_i is the deflection of the spring from its equilibrium position.

The total kinetic energy of the entire system is the sum of the kinetic energies of the links. The total potential energy of the entire system is the sum of the potential energies of the links and also the spring energies; i.e.,

$$K = \Sigma K_i, \tag{14}$$

$$P = \Sigma P_i + \Sigma U_{s_i}. \tag{15}$$

The system has only one degree of freedom, i.e., θ_1, the angular displacement of the crank. It is assumed that the bird is inertially fixed and is oriented at a constant pitch angle θ_a relative to earth. The equation of motion under these conditions is

$$D(\theta_1)\ddot{\theta}_1 + C(\theta_1, \dot{\theta}_1)\dot{\theta}_1 + G(\theta_1) = \tau_{\theta_1}. \tag{16}$$

Here $D(\theta_1)$ is the reflected inertia of the system, $C(\theta_1, \dot{\theta}_1)\dot{\theta}_1$ are quadratic centripetal and nonlinear terms, and $G(\theta_1)$ are the gravity terms [7]. τ_{θ_1} represents the external torques acting on the system.

3 Aerodynamic Model

The aerodynamic model is based on quasi-steady blade element analysis. Here the wing is assumed to be divided into a finite number of strips, each of which are analyzed independently. The span of the wing is assumed rigid; i.e., there is no folding of the wing, unlike that of a bird's wing over a cycle of flapping motion. The unsteady wake effets are accounted for by modified Theodorsen functions [8]. The model includes camber and partial leading edge suction effects. Poststall behavior is also considered in this analysis. In this analysis, the bird is assumed to be inertially fixed in a steady stream of air with the flapping axis pitched up at a constant pitch angle $\bar{\theta}_a$ with respect to the flight speed U.

The kinematics for a section of the wing is represented by a plunging velocity $\dot{h}$ and a pitch angle of the chord θ relative to the free stream velocity (see Fig. 9). The plunging displacement of the leading edge in the flapping direction is defined as [8]

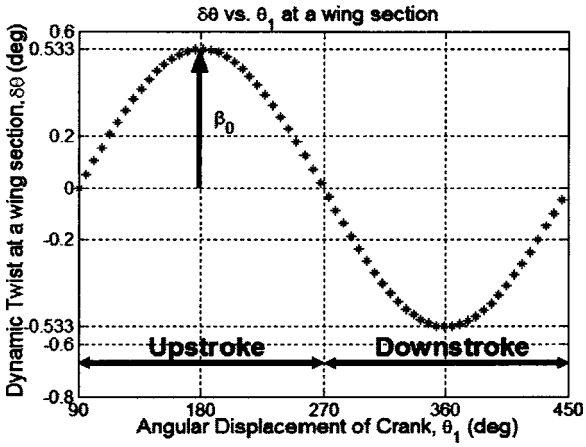

Fig. 10 Variation of $\delta\theta$ with θ_1 at a wing section

$$h = \theta_3 y \tag{17}$$

for the right wing and

$$h = \theta_5 y \tag{18}$$

for the left wing. y is the distance from the root of the wing to the section being analyzed.

The pitch angle of the chord relative to the direction of the flight speed is given by the expression,

$$\theta = \bar{\theta}_a + \bar{\theta}_w + \delta\theta, \tag{19}$$

where, $\bar{\theta}_a$ is the angle made by the flapping axis with respect to the mean-stream velocity, U, $\bar{\theta}_w$ is the mean pitch angle of the chord with respect to the flapping axis (and is assumed zero for a wing with a rigid span) and $\delta\theta$ is the dynamically varying pitch angle defined as

$$\delta\theta = -\beta_0 y \cos\theta_1, \tag{20}$$

where β_0 is the coefficient of the dynamic twist's linear variation along the span of the wing (see Fig. 10) [8].

The forces on each strip are determined solely by the local parameters. The section operates in one of the two distinct flight regimes: stalled or unstalled. This is determined by the relative angle of attack at the leading edge, with the dynamic stall delay effect accounted for [9]. In the unstalled regime of flight, the parameters determining the forces include the section's geometry, relative angle of attack at the 3/4-chord location, pitching rates and the dynamic pressure at the 1/4-chord location. The resulting forces are: (i) dN_c, a force normal to the chord at the 1/4-chord location, (ii) dT_s, a chordwise leading edge suction force, (iii) dD_{camber}, a chordwise drag due to camber, (iv) dD_f, a chordwise drag due to skin friction, and (v) dN_a, an apparent-mass force normal to the chord at the 1/2-chord location. The expressions for the forces on each section are as follows:

$$dN_c = \frac{\rho U V}{2} C_n c\, dy \tag{21}$$

V is the flow's relative velocity at the 1/4-chord location, c is the chord length, ρ is the atmospheric density and

$$C_n = 2\pi(\alpha' + \alpha_0 + \bar{\theta}_a + \bar{\theta}_w) \tag{22}$$

is the normal force coefficient.

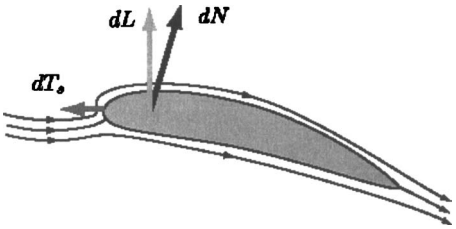

Fig. 11 Leading edge suction effect[10]

$$dN_a = \frac{\rho \pi c^2}{4} \dot{v}_2 dy \tag{23}$$

where $\dot{v}_2$ is the time rate of change of the midchord normal velocity component due to the wing's motion. Therefore, the section's total attached flow normal force is

$$dN = dN_c + dN_a \tag{24}$$

The chordwise force due to camber is

$$dD_{\text{camber}} = -2\pi\alpha_0(\alpha' + \bar{\theta}_a + \bar{\theta}_w)\frac{\rho UV}{2} c dy \tag{25}$$

The sharp diversion of flow around the leading edge causes in a rapid change in the velocity and results in a leading edge suction force, dT_s parallel to the chord (see Fig. 11). This force sums with the normal force vector, dN and causes the resultant force vector, dL, to tilt towards the leading edge and perpendicular to the free stream velocity. This results in an enhancement in the thrust force which is parallel to the free stream [11]. The leading edge suction force is given by the expression

$$dT_s = \eta_s 2\pi\left(\alpha' + \bar{\theta}_a - \frac{c\dot{\theta}}{4U}\right)^2 \frac{\rho UV}{2} c dy \tag{26}$$

The efficiency term, η_a, accounts for the fact that most aerofoils, due to viscous effects, have less than 100% leading edge suction predicted by potential flow theory. Viscosity also gives rise to a chordwise friction drag force given by,

$$dD_f = (C_d)_f \frac{\rho V_x^2}{2} c dy \tag{27}$$

where V_x is the flow speed tangential to the section and $(C_d)_f$ is the drag coefficient due to skin friction. Thus, the total chordwise force is

$$dF_x = dT_s - dD_{\text{camber}} - dD_f \tag{28}$$

In the stalled regime of flight, the key kinematic parameters are the midchord normal velocity component and its derivative, which give rise to the separated flow forces: (i) $(dN_c)_{\text{sep}}$, the midchord cross-chord force, and (ii) $(dN_a)_{\text{sep}}$, an apparent-mass force that is assumed to be 1/2 of dN_a. Also note that in the stalled regime, due to flow separation, the chordwise forces are zero.

$$(dN_c)_{\text{sep}} = (C_d)_{cf} \frac{\rho V_n \hat{V}}{2} c dy \tag{29}$$

$$(dN_a)_{\text{sep}} = \frac{1}{2} dN_a \tag{30}$$

The equations for the segment's instantaneous lift dL and thrust dT are (see Fig. 12)

$$dL = dN \cos\theta + dF_x \sin\theta, \tag{31}$$

$$dT = dF_x \cos\theta - dN \sin\theta. \tag{32}$$

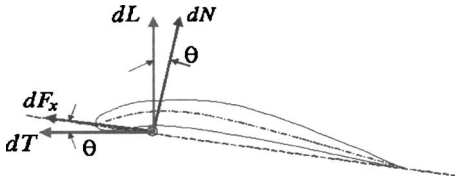

Fig. 12 Chord section showing section lift and thrust forces

The instantaneous lift and thrust for the right wing can be obtained by integrating Eq. (31) and Eq. (32), respectively, over the semi-span of the wing, i.e.,

$$L(t) = \int_0^{b/2} \cos\theta_3 dL \tag{33}$$

$$T(t) = \int_0^{b/2} dT \tag{34}$$

Similarly for the left wing we may write,

$$L(t) = \int_0^{b/2} \cos\theta_5 dL \tag{35}$$

$$T(t) = \int_0^{b/2} dT \tag{36}$$

Here, $b/2$ is the semi-span length.

The segment's aerodynamic moment about the flap axis is given by the expression,

$$dM_{\text{aero}} = (dN\cos(\theta - \bar{\theta}_a) + dF_x \sin(\theta - \bar{\theta}_a))y_i \tag{37}$$

The aerodynamic moments $(M_{\text{aero}})_R$ and $(M_{\text{aero}})_L$ about the flap axes can be obtained by integrating Eq. (37) over the semi-span of each wing. The aerodynamic moment about the crank center due to the forces acting on the right wing is,

$$(M_{a_R})_O = (M_{\text{aero}})_R \frac{\omega_3}{\omega_1} \tag{38}$$

and that about the crank center due to the forces acting on the left wing is,

$$(M_{a_L})_O = (M_{\text{aero}})_L \frac{\omega_5}{\omega_1} \tag{39}$$

Once we have included the aerodynamic model into the system dynamic model the equation of motion becomes,

$$D(\theta_1)\ddot{\theta}_1 + C(\theta_1, \dot{\theta}_1)\dot{\theta}_1 + G(\theta_1) = M_{\text{crank}} + (M_{a_R})_O + (M_{a_L})_O \tag{40}$$

where M_{crank} is the motor torque.

Figure 13 shows the variation of aerodynamic and inertia moments over a cycle of flapping motion. The values of the various parameters, used in the simulation are shown in Table 1 and Table 2. The values of the parameters d_x and d_y are 0.15 m and 0.21 m, respectively. As is evident from the plots the the aerodynamic moment is considerably more compared to the inertia moment. Also, the aerodynamic moment during the downstroke is more than that during the upstroke. This is due to the fact that the downstroke is the power stroke, whereas the upstroke is the recovery stroke. The aerodynamic forces are greater during the downstroke and hence the moment due to these forces are also greater. The motor needs to overcome the moment produced during both the strokes to maintain the required lift. Figure 14 shows the lift and thrust generated by both the wings during one complete cycle of flapping motion. The average lift and thrust are

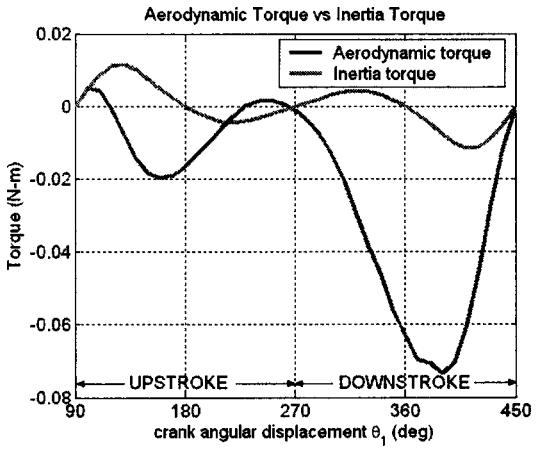

Fig. 13 Variation of aerodynamic and inertia moments over a cycle of flapping motion

found to be 0.4568 N and 0.0675 N, respectively. It can be seen that the lift force balances the weight of the bird which is 46 g and there is a net positive thrust.

The values of the aerodynamic constants shown in Table 2 must satisfy the conditions for cruise flight which are:

- The average lift over a cycle of flapping motion should be greater than or equal to the weight of the bird.
- The average thrust must be positive.
- The propulsive efficiency must lie between 0 and 1.

The value of β_0 was arrived at by plotting the average lift, average thrust and propulsive efficiency over a range of β_0 values

Table 1 Values of the lengths and masses of the links

Parameter	Crank (l_1)	Coupler (l_2)	Rocker (l_3)	Wing (l_4)
Length (m)	0.006	0.02	0.015	0.33
Mass (kg)	0.25×10^{-3}	0.0005	0.00025	0.0025

Table 2 Values of aerodynamic constants

β_0(deg/m)	θ_a(deg)	U(m/s)	ρ(kg/m^3)	f(Hz)
52.4934	4	5	1.225	3.5

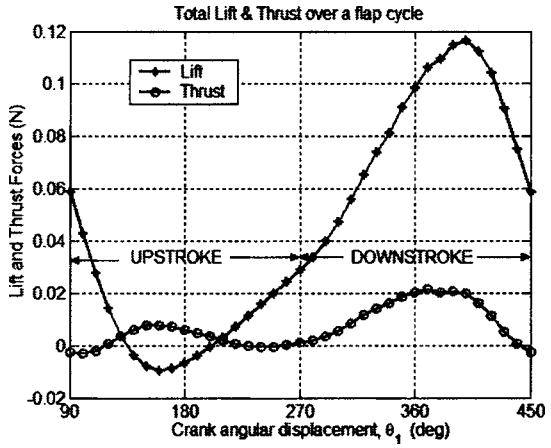

Fig. 14 Variation of total lift and thrust over a cycle of flapping motion

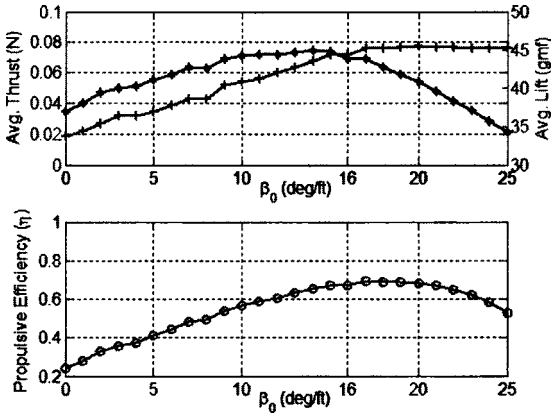

Fig. 15 Selection of β_0

(see Fig. 15). The value of β_0 that was chosen (approximately 16 deg/ft=52.4934 deg/m) satisfies the conditions for optimal flight mode. In addition, from Fig. 15, it can be observed that beyond this value of β_0 the thrust and propulsive efficiency begin to decrease. Choosing the values of $\bar{\theta}_a$ and f as shown in Table 2, we find the value of flight speed, U, that satisfies the conditions for cruise flight (see Fig. 16).

4 Optimization of Design

Results obtained in the previous section have shown that the magnitude of aerodynamic moments is considerable during a cycle of flapping motion. In addition, the moment during the downward power stroke is more than that during the upstroke which is the recovery stroke. At the end of each stroke the wings decelerate to a stop and reverse direction. This causes the aerodynamic moments to vanish at the end of the stroke. At the beginning of the next stroke the wings accelerate from rest, due to which they encounter very high forces and hence moments. The consequence being that the drive motor experiences a sharp variation of aerodynamic torque over a cycle of flapping motion. Our proposal is to incorporate tension springs of appropriate free length l_0 and stiffness k_s at appropriate distance r (see Fig. 5) into the design. These springs can reduce the variation in the load torque over a cycle, thereby keeping the peak values of the load torque low. This will also prevent the motor from experiencing *shock*, or sharp variation in torque during a cycle of flapping motion.

The springs are so attached that they are unstretched during the start of the upstroke and fully stretched at the end of the upstroke (or beginning of the downstroke). The stretching of the spring

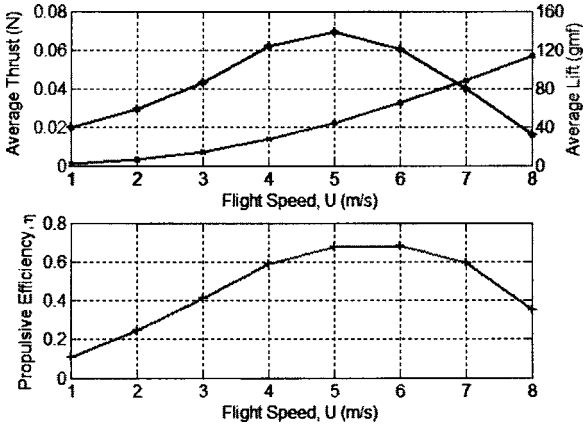

Fig. 16 Value of *U* satisfying optimal flight conditions

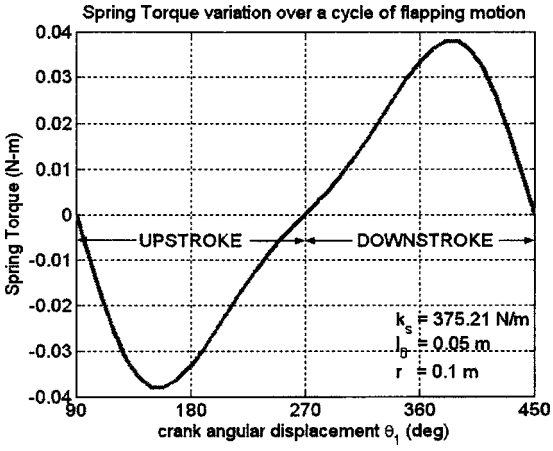

Fig. 17 Variation of spring torque over a cycle of flapping motion

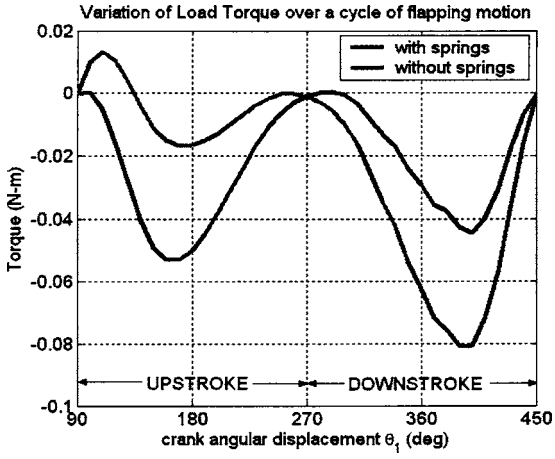

Fig. 18 Comparison of variation of load torque over a cycle for a system with and without springs

causes a reaction force and the moment due to this force acts against the motor thereby increasing the torque during the upstroke. During the downstroke, the stretched springs tend to pull the wings down, thereby aiding the motor and decreasing the moment during the downstroke (see Fig. 17). For a particular size of the bird, the spring free length cannot exceed a optimum value. This is because, if the free length is too high then the point of attachment of the spring along the wing's leading edge will increase. This in turn will increase the moment due to the spring force. Since, the spring acts against the motor during the upstroke, it may cause the moment to increase beyond a reasonable value. Also, the moment during the downstroke will be reduced greatly. The result is that the sharp variation in the load torque is not reduced and hence the purpose of incorporating springs is lost.

Static optimization technique [12] is made use of to determine the optimum free length l_0, stiffness k_s of the tension spring and optimum distance r from fixed point C. The load torque is given by the expression,

$$M_{\text{load}} = M_{\text{inertia}} + M_{\text{aero}} + M_{\text{spring}} \tag{41}$$

where M_{spring} is the spring torque. The cost function is given by the expression,

$$F = M_{\max} - M_{\text{avg}} \tag{42}$$

where $M_{\max}$ is the peak torque over a cycle and M_{avg} is the average torque over the cycle. By minimizing the above cost function we can minimize the variation in the load torque. This way the we can prevent the motor from experiencing sharp variation in the torque.

The fmincon() function in MATLAB has been made use of to perform the optimization of the design. This function finds a constrained minimum of a scalar function of several variables starting at an initial estimate. This is generally referred to as *constrained nonlinear optimization or nonlinear programming*. The initial guesses and bounds for the stiffness (k_s), free length (l_0), and point of attachment (r) of the spring respectively are given in Table 3.

The optimum values for the spring stiffness k_s, free length l_0, and distance of point of attachment r of the spring along the wing's leading edge from fixed point C were found to be 375.21 N/m, 0.05 m, and 0.1(m), respectively. Using these optimum values in the simulations we obtain the following results. Figure 18 compares the variation of load torque for a system with springs and for a system without springs. It is evident from the figure that the addition of springs of appropriate free length and stiffness at an appropriate point on the leading edge does indeed reduce the variation of the load torque over a cycle of flapping motion. The percentage reduction in the variation was found to be 56.32%.

Table 3 Initial guesses and bounds for design optimization

Parameter	k_s(N/m)	l_0(m)	r(m)
Initial guess	100	0.04	0.04
Lower bound	0	0.01	0.05
Upper bound	500	0.1	0.2

Conclusion

The study of flapping wing machines is an interesting and challenging problem. In this paper, we have presented an energetics-based design of a mechanical flapping wing machine that significantly reduces the peak torque and hence the peak input power requirement of the drive motor. This was motivated from the study of insect flight in which the thorax of the insect acts as an energy storage unit, storing the kinetic energy of the wings as elastic potential energy and releasing this energy during the subsequent stroke. This way the work done by the muscles which need to drive the wings from rest at the start of every stroke, is reduced considerably. Analogous to the insect thorax, our design makes use of tension springs which are so attached that they increase the torque during the upstroke and reduce the same during the downstroke thereby reducing the sharp variation in the torque over the entire cycle and keeping its value within the peak torque requirements of the drive motor. Since the angular velocity of the crank is assumed to be constant, a reduction in the peak torque requirement is proportional to a reduction in the peak input power requirement of the drive motor. The model of the system includes both inertia effects, gravity effects and aerodynamic effects.

Acknowledgment

This work is being supported by the AFRL/MNK Grant, award number F08630-03-C-0195.

References

[1] Pornsin-Sirirak, T. N., Tai, Y. C., Nassef, H. and Ho, C. M., 2001, "Titanium-alloy MEMS Wing Technology for a Micro Aerial Vehicle Application," Sens. Actuators, A, **89**, Issue 1–2, pp. 95–103.

[2] Jones, K. D. and Platzer, M. F., 1999, "An Experimental and Numerical Investigation of a Flapping Wing Propulsion", 37th AIAA Aerospace Sciences Meeting, AIAA paper No. 99-0995.

[3] C. P. Ellington, 1984, "The Aerodynamics of Hovering Insect Flight I. The Quasi-Steady Analysis," Philos. Trans. R. Soc. London, Ser. B, **305**, pp. 1–15.

[4] Sane, S. P., and Dickinson, M. H., 2002, "The aerodynamic effects of wing rotation and a revised quasi-steady model of flapping flight," J. Exp. Biol., **205**, pp. 1087–1096.

[5] Dalton, S., 1977, *The Miracle of Flight*, McGraw-Hill Book Company, New York, p. 43.
[6] Ellington, C. P., 1984, "The aerodynamics of hovering insect flight. VI. Lift and power requirements," Philos. Trans. R. Soc. London, Ser. B, **305**, No. 1122, pp. 145–181.
[7] Spong, M. W., and Vidyasagar, M., 1989, *Robot Dynamics and Control*, John Wiley & Sons, New York, p. 129.
[8] DeLaurier, J. D., 1993, "An Aerodynamic Model for Flapping-Wing Flight," Aeronaut. J., **97**, No. 964, pp. 125–130.
[9] DeLaurier, J. D., 1994, "An Ornithopter Wing Design," Can. Aeronautics Space J., **40**(1), pp. 10–18.
[10] Sane, S. P., 2003, "The aerodynamics of insect flight," J. Exp. Biol., **206**, pp. 4191–4208.
[11] Dickinson, M. H., and Gotz, K. G., 1993, "Unsteady Aerodynamic Performance Of Model Wings At Low Reynolds Numbers," J. Exp. Biol., **174**, pp. 4564.
[12] Agrawal S. K., and Fabien B. C., 1999, "Optimization of Dynamic Systems," Kluwer Academic Publishers, Dordrecht.